Eur. Phys. J. D **20**, 121–127 (2002)
DOI: 10.1140/epjd/e2002-00108-1

THE EUROPEAN PHYSICAL JOURNAL D

Coupled longitudinal and transverse stimulated Brillouin scattering in single-mode optical fibers

I. Bongrand[a], É. Picholle[b], and C. Montes

CNRS, Laboratoire de Physique de la Matière Condensée, Université de Nice-Sophia Antipolis, Parc Valrose, 06108 Nice Cedex, France

Received 17 September 2001 / Received in final form 5 March 2002
Published online 28 June 2002

Abstract. Due to their finite numerical aperture, both longitudinal and transverse stimulated Brillouin scattering can occur in single-mode fibers. We discuss the role of the fiber structure and propose a coherent model accounting for both effects. We show experimentally and numerically that, in some cases, the perturbative cladding Brillouin scattering (CBS) can severely affect the dynamics of SBS Brillouin fiber lasers. New dynamical regimes of long-fiber Brillouin ring lasers are presented, including stable trains of modulated pulses.

PACS. 42.65.Es Stimulated Brillouin and Rayleigh scattering – 42.81.Dp Propagation, scattering, and losses; solitons – 42.25.Gy Edge and boundary effects; reflection and refraction

1 Introduction

The nonlinear dynamics of Brillouin fiber lasers stands among the richest and most various in Optics. Under the one-dimensional approximation customary in single-mode fibers, it is now fairly well understood in the frame of the coherent 3-wave model of stimulated Brillouin scattering (SBS) [1,2], which accounts for perturbative optical Kerr effect and spontaneous noise [3]. Such Brillouin devices exhibit periodic, quasi-periodic [4–7], chaotic [8] and even solitonic super- and sub-luminous pulse propagation [9,10], as well as self-stabilisation of the phase yielding ultracoherent regimes (thus linewidths as narrow as a few hertz [11,12]). Yet, they are fairly simple to operate, due to the very high gain easily achievable with only tens of mW of pump power in long enough single-mode fiber, which allows very low finesses and reinjection rates.

It should nevertheless be kept in mind that single-mode optical fibers actually have finite numerical apertures. Moreover, "single-mode" optical fibers also behave as highly *multimode* acoustic waveguides. An optical beam can thus be scattered at a non-zero angle from the fiber axis, and yet remain fully guided if this angle is small enough. While SBS conventionally refers in fibers to the *back*scattering ($\theta = \pi$) of light by an axial acoustic wave, the small-angle effect concerns its "forward" scattering on acoustic waves propagating radially on the fiber's cladding (from now on, we will design such acoustic waves as "transverse", in a geometrical sense, even when their polarization is longitudinal). This transverse Brillouin effect is thus designed as "cladding Brillouin scattering" (CBS). It is sometimes referred to as the "electrostriction mechanism" or the "acoustic interaction" in the context of optical telecommunications [13,14], or as spontaneous "guided-acoustic-wave Brillouin scattering" (GAWBS) in quantum optics [15], and CBS-induced passive mode-locking of fiber lasers has been reported [16,17].

In Brillouin fiber lasers, low-frequency CBS-scattered satellites of the Brillouin signal fall under the SBS gain curve, yielding new dynamical features [18]. In this paper, we propose a simple quasi-1D model of the Brillouin interaction in single-mode fibers, taking into account their finite numerical aperture and both longitudinal (SBS) and transverse (CBS) processes. We discuss their relative efficiencies and give analytical expressions of the relevant overlap integrals. We show experimentally that, in some cases, the transverse perturbation can severely affect the dynamics of long fiber Brillouin lasers, in very good qualitative agreement with the numerical simulations of our coherent model.

2 Finite numerical aperture and quasi-1D Brillouin process

The elementary Brillouin process can be described as a 3-wave interaction, a "forward" optical "pump" wave (ω_p, $\mathbf{k}_\mathrm{p}$; $k_\mathrm{p} = n\omega_\mathrm{p}/c$) being scattered onto an optical "Stokes" wave (ω_s, $\mathbf{k}_\mathrm{s}$) through its interaction with an acoustical wave (ω_a, $\mathbf{k}_\mathrm{a}$; $k_\mathrm{a} = \omega_\mathrm{a}/c_\mathrm{a}$) created by electrostriction.

[a] *Present address*: Alcatel R&I, Unité Fibres et Composants, 91461 Marcoussis, France.
[b] e-mail: `eric.picholle@unice.fr`

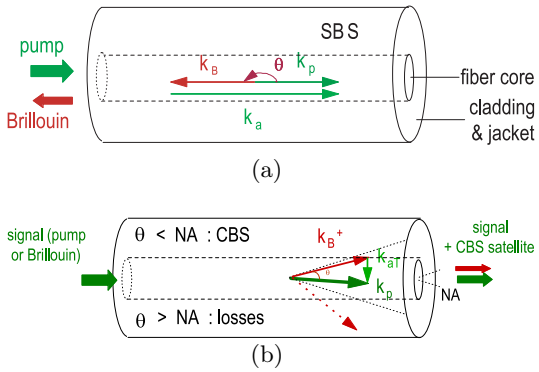

Fig. 1. (a) Phase matching diagram for Brillouin backscattering ($\theta = \pi$, 1D SBS case). (b) Phase matching diagram for transverse Brillouin scattering ($|\theta| < NA$, CBS case). A symmetric diagram describes CBS on the "backward" waves ($|\pi - \theta| > NA$).

In bulk media, it takes place in every direction, the energy and impulsion conservation laws ($\omega_\mathrm{a} = \omega_\mathrm{p} - \omega_\mathrm{s}$, $\mathbf{k}_\mathrm{a} = \mathbf{k}_\mathrm{p} - \mathbf{k}_\mathrm{s}$) yielding $\omega_\mathrm{a} = \omega_\mathrm{a}^0 \sin\theta/2$, where θ is the scattering angle between the two optical beams and $\omega_\mathrm{a}^0 = 2nc_\mathrm{a}/c\,\omega_\mathrm{p}$ is the backscattering frequency shift. Obviously, in an optical fiber with a finite numerical aperture NA, whenever $|\theta| > NA$ and $|\pi - \theta| > NA$, this corresponds to overall additional optical losses typically amounting to about 1% of the usual propagation losses (Fig. 1). Here, electrostriction can be seen as the tendency of dielectric matter to escape intensity gradients, either longitudinal (interference patterns between co- and counter-propagating optical waves) or transverse (optical mode profile).

Let us first consider the usual SBS backscattering case. In a typical single-mode fiber, this calls for very high acoustic frequencies, typically $\omega_\mathrm{a}^0/2\pi = 33$ GHz (for $\lambda_\mathrm{p} = 532$ nm, $\theta = \pi$) and thus very short acoustic wavelengths ($\lambda_\mathrm{a} = 170$ nm). The acoustic wavevector is mostly axial (Fig. 1a) and the interaction thus involves longitudinally polarized acoustic waves guided in the core region of the fiber, which behaves as a multimode acoustic waveguide (or anti-waveguide for some doping materials). Only a scarce number of acoustic modes are available; since the SBS gains depending on their overlap with the optical modes, only the fundamental is relevant for acoustically guiding fibers. The spectral width of the backscattered wave basically depends on the acoustic losses of these individual modes, to which may be associated an effective damping parameter.

The problem is somewhat more complicated in the transverse CBS case (Fig. 1b). The involved acoustic waves now propagate radially in the whole fiber structure (core + cladding + jacket), whose transverse section can be considered as a resonator with a fundamental resonant frequency typically around 4 MHz [19]. The optical guiding condition ($|\theta| < NA$) yields an acoustic cutoff frequency $\omega_\mathrm{a}^\mathrm{max} \approx \omega_\mathrm{a}^0 NA/2$ in the GHz range ($\omega_\mathrm{a}^\mathrm{max}/2\pi \approx 1.7$ GHz @ 532 nm for $NA = 0.1$). The dominant losses are the almost frequency-independent reflections at the cladding/jacket and jacket/air interfaces [20], the acoustic propagation damping ($\propto \omega_\mathrm{a}^2$) being relevant only in the GHz range and above [21,22]. The CBS-active radial (R_{0n}) and torso-radial (TR_{2n}) acoustic modes are easy to determine analytically as long as the fiber has a cylindrical symmetry and can be considered homogeneous [15], but no general solution is available, and even numerical computations call for heavy hypothesis in the inhomogeneous case. Both axial (SBS) and radial compressive acoustic waves of velocity c_a ($c_\mathrm{a} = v_l^\mathrm{cl} \approx 5\,960$ m/s in the silica cladding) are longitudinally polarized with respect to their propagation direction, while the deformation associated to the torso-radial modes is normal to their propagation, yielding a "shear" velocity v_s^cl ($\approx 3\,740$ m/s).

3 Evolution equation for radial acoustic waves

Since CBS acoustic waves propagate radially and we are only interested on their behaviour in the core region of the fiber, we can describe them through a single parameter, namely the material density variation in the small core region due to electrostriction. This noninstantaneous material response can then be directly incorporated into the evolution equation for the optical waves [23]; here, we will rather account for it in a separated evolution equation, following the usual approach developed for SBS. The acoustic power is always very small, thus the propagation of the acoustic waves remains linear [24] and any acoustical excitation created through electrostriction can be decomposed over a complete set of orthogonal modes [13] (some of them lossy) with complex amplitude ρ_n and normalized and dimensionless transverse profiles M_n; the material density thus reads:

$$\rho(r,\varphi,z,t) = \rho_0 + \sum_n \rho_n(z,t) M_n(r,\varphi) \exp[-\mathrm{i}(\Omega_n t)] + \text{c.c.}$$

To account for the transverse acoustic modal structure of the fiber, we describe locally each CBS transverse acoustic mode of frequency Ω_n and damping γ_n through a standard damped and forced harmonic oscillator equation:

$$\left[\partial_{tt} + 2\gamma_n\partial_t + \Omega_n^2\right] \rho_n(z,t) = -\kappa_{n\perp} |E(z,t)|^2 + f_n(z,t) \tag{1}$$

f_n is a Langevin noise term [3]. The optical intensity I is related to the electrical field through: $I = P/a_\mathrm{eff} = (n_\mathrm{eff}\varepsilon_0 c/2)|E|^2$. In a SBS laser, both pump and Brillouin waves, of intensities $I_\mathrm{p,B}$, independently participate to the excitation of the transverse acoustic modes: $I = I_\mathrm{p} + I_\mathrm{B}$.

The validity of the phenomenological equation (1) is quite general, as far as the diameter of the optical mode remains much smaller than the acoustic wavelength (typ. $\Omega_n \ll 1$ GHz). In ideal homogeneous fibers where only pure rod modes are available, the direct electrostrictive excitation of acoustical shear waves (TR_{2n}) depends on the polarisation state of the optical beams, with $\kappa_{n\perp}^\mathrm{shear}$ vanishing for linear polarizations [25], while longitudinal waves (R_{0n}) are mostly polarization insensitive.

Its general derivation in coated fibers would call for a rather complex discussion of the coupling between compressive and shear acoustic waves at the fiber boundaries, which strongly depends on the acoustic impedance at the cladding/jacket interface, and should take into account the dielectric permeability changes associated to the strain tensor changes. The complete map of the mechanical properties of the inhomogeneous fiber is seldom available, and this difficult problem of elasticity theory is far beyond the scope of this article; we will thus consider, when necessary, only empirical values for $\kappa_{n\perp}^{\text{shear}}$ (which, in our experiment with a severely inhomogeneous fiber, appears to be of the same order of magnitude than the $\kappa_{n\perp}$ obtained for all low-frequency R_{0n} modes).

On the other hand, a much simpler hydrodynamical approach of the density variations in silica glasses remains valid when only compressional waves are involved; it allows a straightforward derivation of equation (1) from the fundamental laws of motion [1] for the compressive (R_{0n}) CBS modes, through $\partial_t \rho - \rho_0 \boldsymbol{\nabla} \cdot \partial_t \mathbf{u}_l$. Only two forces are to be taken into account, namely, for a cylindrical fiber, a radial electrostrictive pressure

$$\mathbf{f}_{\text{r}}^{\text{el}} = \frac{\partial \varepsilon}{\partial \rho} \frac{\rho_0 \varepsilon_0}{2} \boldsymbol{\nabla}_\perp \left| E^2 \right|$$

and a friction $\mathbf{f}_{\text{r}}^n = 2\gamma_n \mathbf{u}_{\text{r}}$ to which, for simplicity, we will artificially incorporate as distributed losses the reflection losses at the cladding/jacket and jacket/air interfaces (thus $\gamma_n \approx \pi \times 2$ MHz [20]). Remembering that M_n is a solution of the free acoustic propagation equation in the fiber, and taking into account the transverse profile $F(r, \varphi)$ of the (one) optical mode, the integration over the fiber section yields equation (1), with

$$\kappa_{n\perp} = \frac{\rho_0 \varepsilon_0}{2} \frac{\partial \varepsilon}{\partial \rho} B_n^{\Delta}. \tag{2}$$

The expression of B_n^{Δ} is given in Appendix A, together with all other overlap integrals B_i. Let us emphasize that, due to the transverse Laplacian it involves, its value, hence the efficiency of CBS, might vary over several orders of magnitude depending on the actual optical mode profile; it would even vanish for an homogeneous acoustic mode profile and a symmetrical optical mode profile in a perfectly cylindrical fiber with infinite cladding [26]. The Lorentz–Lorenz relation yields:

$$3\rho_0 \frac{\partial \varepsilon}{\partial \rho} = \left(n^2 - 1\right)\left(n^2 + 2\right).$$

Simple hypothesis (homogeneous silica rod, Lorentzian modes) yield $\kappa_{n\perp} \approx 1 \times 10^{14}$ kg m^{-1} s^{-2} V^{-2} for all low-order radial modes (R_{0n}, $\Omega_n \ll 1$ GHz). Available measurements [20,21], including our own, suggest that this value is typically underestimated by two orders of magnitude. This calls for a more detailed, and rather difficult, analysis of the optical [27] as well as acoustical mode profiles, taking into account the small density and composition gradients in the core region.

When strictly monochromatic optical beams are involved, as in fiber quantum optics experiments, it can be relevant to distinguish separate carriers for the pump wave and its copropagating scattered satellites with a frequency difference Ω_n (whose beating thus induce an additional resonant excitation of the acoustic mode [14]). The statistical properties of the noise term f_n is then of prime importance, and can be derived experimentally [20] or from thermodynamical considerations [28,29].

4 Coherent model for coupled longitudinal and transverse Brillouin processes

Here, we are interested in spectrally larger beams. In the slowly varying optical envelope approximation, the nonlinear density variations associated to the transverse acoustic wave can be interpreted as a perturbative non-instantaneous Kerr-like contribution to the optical index. It is thus straightforward to generalize the usual coherent 3-wave model of SBS [1]. The evolution equations for the pump and Brillouin envelopes (from now on, by "Brillouin" we will design the backward propagating SBS-scattered Stokes wave) thus read:

$$\left[\partial_t + \frac{c}{n_{\text{eff}}}\partial_z + \gamma_e\right] E_{\text{p}} = \text{i}\,\kappa^{\text{SBS}} E_{\text{B}}\,\rho_{\text{a}} + \text{i}\sum_n \kappa_n^{\text{CBS}} E_{\text{p}}\,\rho_{\text{n}} + \text{i}\,\kappa^{\text{Kerr}}\left(\left|E_{\text{p}}\right|^2 + 2\left|E_{\text{B}}\right|^2\right) E_{\text{p}} \tag{3}$$

$$\left[\partial_t - \frac{c}{n_{\text{eff}}}\partial_z + \gamma_e\right] E_{\text{B}} = \text{i}\,\kappa^{\text{SBS}} E_{\text{p}}\,\rho_{\text{a}}^* + \text{i}\sum_n \kappa_n^{\text{CBS}} E_{\text{B}}\,\rho_{\text{n}} + \text{i}\,\kappa^{\text{Kern}}\left(2\left|E_{\text{p}}\right|^2 + \left|E_{\text{B}}\right|^2\right) E_{\text{B}} \tag{4}$$

where $E_{\text{p,B}}$ are the complex amplitudes of the pump and Brillouin optical fields, γ_e the optical losses, and n_{eff} the effective refractive index of the fiber. ρ_{a} is the complex amplitude of the slowly varying envelope of the usual high frequency SBS longitudinal acoustic wave of frequency ω_{a}^0 and damping $\gamma_{\text{a}} = \pi \Delta\nu_{\text{B}}$. The Kerr coupling constant is related to the effective (automodulation) nonlinear index n_2 through

$$\kappa^{\text{Kerr}} = \frac{n_2 \omega_{\text{p}}}{2n} B^{\text{Kerr}}.$$

The electrostrictive coupling constants κ^{SBS} and κ_n^{CBS} read:

$$\kappa^{\text{SBS}} = \frac{\omega_{\text{p}}}{4n_{\text{eff}}^2} \frac{\partial \varepsilon}{\partial \rho} \sqrt{\frac{c_{\text{a}}}{c_{\text{a}}^{\text{eff}}}} B^{\text{SBS}} \tag{5}$$

$$\kappa^{\text{CBS}} = \frac{\omega_{\text{p}}}{2n_{\text{eff}}^2} \frac{\partial \varepsilon}{\partial \rho} B^{\text{SBS}}. \tag{6}$$

The core of the fiber constitutes a weak acoustic waveguide (or antiwaveguide) for the high frequency, longitudinally

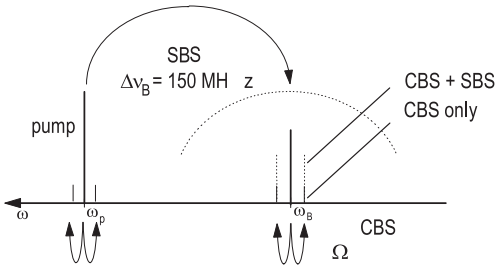

Fig. 2. Schema of electrostrictive energy transfers in a single-mode fiber: the strongest effect is the resonant SBS coupling between the forward pump ($\omega_{\rm p}$) and backward Stokes ($\omega_{\rm B}$) waves; CSB induces satellites to each wave ($\pm\Omega$), without changing their direction; CSB satellites of the Stokes wave fall into the SBS gain curve ($\Delta\nu_{\rm B} \gg \Omega$) [SBS-enhanced CBS] and are thus much stronger than those of the pump wave.

polarized axial acoustic wave $\rho_{\rm a}$. Only its fundamental mode, of effective velocity $c_{\rm a}^{\rm eff}$ and for which $B^{\rm SBS} \approx 1/2$, is to be considered. Higher order modes yield vanishing overlap integrals [30,31]. The amplitude of this mode follows:

$$\left[\partial_t + c_{\rm a}^{\rm eff}\partial_z + \gamma_{\rm a}\right]\rho_{\rm a} = {\rm i}\,\kappa_{\rm a}\,E_{\rm p}\,E_{\rm B}^{*} + f_{\rm a}(z,t) \qquad (7)$$

where

$$\kappa_{\rm a} = \frac{n_{\rm eff}\omega_{\rm p}\rho_0\varepsilon_0}{4c\,c_{\rm a}^{\rm eff}}\frac{\partial\varepsilon}{\partial\rho}B_{\rm a}. \qquad (8)$$

When only one CBS mode is involved, the dynamics of the coupled SBS and CBS problem in fiber is thus described by the quasi-1D 4-wave coherent model constituted by equations (3, 4, 7, 1), which can be expressed in dimensionless variables involving only two (Kerr & CBS) parameters (see Appendix B). The generalization to a $(n+3)$-wave model n CBS modes is obvious, as well as the reduction to a one-mode pure CBS problem ({NLS equation + (1)} [14]); nevertheless, a Green function approach [32] is more tractable numerically for many CBS modes, although difficult to implement with counterpropagating optical beams (thus in the SBS case).

Although the same electrostriction mechanism governs both SBS and CBS, the efficiency of the former is much higher, typically by two orders of magnitude. This is due to the better overlap between the optical modes and the core-confined SBS acoustical waves (purely geometric) than with the cladding-spread CBS modes (Laplacian).

5 Perturbed long-fiber SBS laser

In a SBS fiber laser, CBS will thus appear as a perturbative effect and can usually be neglected. Nevertheless, it affects both the pump and Brillouin waves, creating satellites in their spectra. Such satellites can no longer be neglected when they affect the Brillouin wave and fall into the SBS gain curve of width $\Delta\nu_{\rm B}$ (Fig. 2): low-frequency CBS can then be strongly enhanced through its coupling with SBS [33]; this mechanism is similar to the so-called

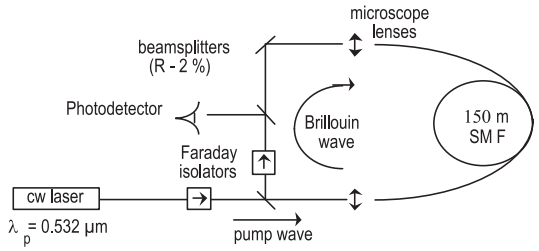

Fig. 3. Experimental setup.

"Brillouin enhanced four-wave mixing" involving the coupling between SBS and the optical Kerr effect [34]. In order to validate our coupled CBS/SBS model (and more generally our coherent description of CBS), we will thus compare its numerical simulation with an experiment in a Brillouin fiber ring laser pumped by a 5 W cw pump laser at $\lambda_{\rm p} = 532$ nm, yielding $\Delta\nu_{\rm B} \approx 150$ MHz. We use a basic mirror-and-lens setup, with and intracavity Faraday isolator to prevent launched intensity fluctuations related to the recoupling of the pump wave (Fig. 3).

Since this design was first proposed in the early 70s [35], the amazingly rich dynamics of Brillouin fiber ring lasers has been characterized in almost every possible configuration. Basically, for a given launched pump power, it is determined by two key parameters: the fiber length L (actually the number of modes available under the SBS gain curve, $N = \Delta\nu_{\rm B}nL/c$, [2]) and the Brillouin feedback parameter R [6]. Short-fiber Brillouin lasers ($N \approx 1$, or $L < 10$ m, typically) are intrinsically continuous (cw) devices [7] of very high coherence [11]. Longer fibers ($N \approx 30{-}60$) yield either cw outputs for high R, or stable pulsed outputs in the low finesse regime (typ. $R < 0.1$). Both types are mostly insensitive to third-order effects, such as Kerr or CBS perturbations, except in the unstable bifurcation region between pulsed and steady regimes [33]. Very long devices ($N > 100$), on the other hand, are quite sensitive to any perturbation, which allows us to study the SBS/CBS coupling.

Our active medium will thus be a 150 m ($N \approx 110$) single-mode fiber (*Spectran* A0515B). We discuss elsewhere [19] the influence of its jacket on the CBS-mode structure of this non polarization preserving fiber of effective area $a_{\rm eff} \approx 45 \times 10^{-12}$ m^2, with 24 dB/km attenuation @ 514.5 nm ($\gamma_e = 5.6 \times 10^5$ s^{-1}). A low feedback ($R \approx 0.01$) yields pulsed regimes for moderate pump intensities. This compromise allows to consider that only one longitudinal cavity mode falls into a given CBS gain curve ($FSR \approx 1.36$ MHz; $\gamma_n/\pi \approx 2$ MHz), while an even longer device ($FSR \ll \gamma_n$) would have a more complicated dynamics. Even so, several CBS resonances can be simultaneously excited, but such regimes appear to be rare, and typical FFT spectra of the Brillouin signal show only one significant CBS resonance one order of magnitude higher than those of the other resonances, whenever a severely perturbed regime is attained.

We will thus focus our analysis on such regimes, different enough from the unperturbated SBS dynamics for the identification of the perturbation to be unambiguous,

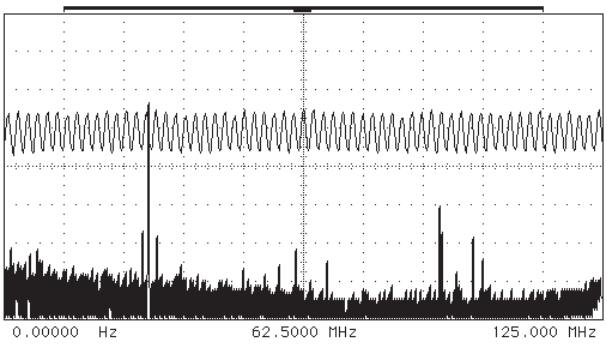

Fig. 4. 24 MHz oscillation over the SBS mirror & FFT spectrum (Stokes wave, experimental).

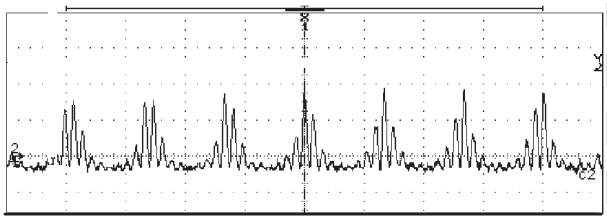

Fig. 5. Stable modulated structures (Stokes wave, experimental).

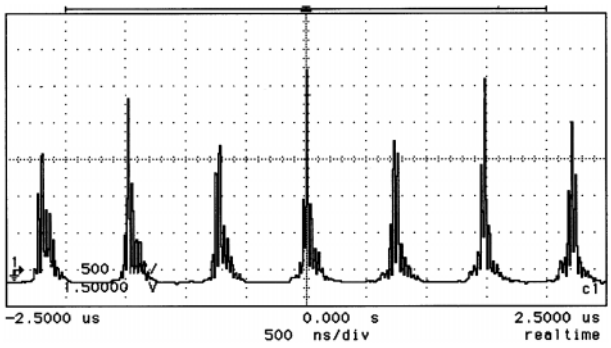

(a)

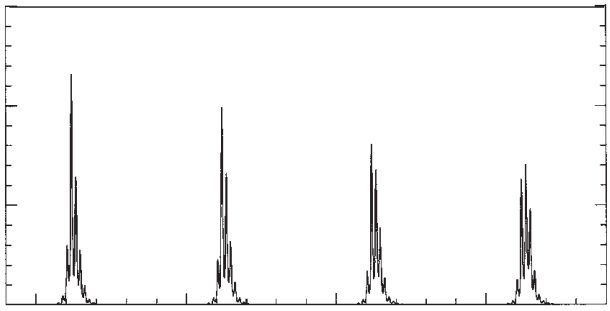

(b)

Fig. 6. High peak-intensity transitories: (a) Stokes wave, experimental; (b) 4-wave SBS/CBS model, numerical.

and which allows us to limit our simulations to a 4-wave problem. Numerically, we adopt the quasi-1D 4-wave model described in Appendix B for various CBS resonances, and use a four-step Runge-Kutta algorithm to describe the spatio-temporal interaction ($c_{\rm a}^{\rm eff} \ll c$). We take $\kappa_{\rm a}^{\rm SBS} = 50\ {\rm m\,s^{-1}\,V^{-1}}$, $\kappa^{\rm Kerr} = 2\times10^{-3}$, $\gamma_{\rm a} = \pi\times150$ MHz [2] and $\gamma_n = \pi\times2$ MHz. $\kappa_n^{\rm CBS}$ varies from 10^{-3} to 6×10^{-2}, mainly depending on the overlap integral B_n^{Δ} given by (A.1). Nevertheless, above a critical $\kappa^{\rm CBS}$, we have shown [18] that the dynamical behavior becomes less sensitive to the coupling parameter than to the detuning between Ω and the nearest longitudinal mode of the laser. The critical perturbative value ($\approx10^{-3}$) is however greater by two orders of magnitude than that obtained by evaluating B_n^{Δ} for the simplest symmetrical radial acoustic mode in standard fibers.

The simplest perturbed regime is an oscillation over the cw SBS mirror (Fig. 4), at the frequency of the first CBS modes ($\Omega = 5{-}25$ MHz, or $4{-}20FSR$), instead of the first and second modes ($\omega/2\pi = FSR$ or $2FSR$) solely observed in shorter devices during the regular Hopf bifurcation towards the quasi-solitonic 3-wave regime [2,6]. Here, these "bare" SBS solitons (typically 28 ns FWHM) leave place either to compressed or dilated (18–75 ns) unmodulated pulses [18], or to evolutive modulated structures. Low CBS frequencies yield very large (typ. 100 ns) and rather stable modulated Brillouin structures (Fig. 5); higher modulation frequencies ($\Omega\times28$ ns > 1) yield less stable short pulses of very high maximum amplitude (up to 15 times the pump power), as shown in Figure 6a. These features are in excellent qualitative agreement with the numerical simulations (Fig. 6b). Note that the phase velocity of the modulation is different from the signal velocity.

6 Conclusion

For almost three decades, stimulated Brillouin scattering has been one of the most widely studied process in single-mode fibers, either as a detrimental effect to be avoided in optical telecommunications or, from a more fundamental point of view, as one of the very few nonlinear and noninstantaneous effects whose dynamics could be entirely followed, experimentally and theoretically, from its emergence from a shapeless initial noise up to stable dynamical asymptotic stages [2]. These results have been obtained under the very strong one-dimensional approximation, which now appears to be consistent only for short enough interaction lengths. Transverse Brillouin effects have been known to appear in very-long span ($10^5{-}10^7$ m) fibers used in telecommunication systems [13], but we have shown in the present paper that they may also severely affect the dynamics of Brillouin lasers for fiber lengths in the 10^2 m range. We have proposed a quasi-unidimensional 4-wave (or $[3+n]$-wave) model taking into account both longitudinal and transverse Brillouin scattering in single-mode fibers, which appeared in excellent qualitative accordance with the experiments. We have also emphasized the need of a precise characterization of both optical and acoustical mode profiles to define *a priori* the efficiency of the CBS process that, unlike SBS's, can vary over several orders of magnitude from one fiber to another.

Obviously, the dynamics of the complete problem, SBS + CBS – namely, a resonant 3-wave nonlinear

process, with a noninstantaneous response in the ns range, itself nonlinearly coupled to an independent oscillator whose period lies in the μs range, is bound to be all the more complicated. Surprisingly enough, we found that even a perturbative coupling could, in some conditions, yield new and rather stable dynamical regimes, namely strongly modulated Brillouin pulses, both fully different from the regular quasi-solitonic regime, and rather stable. This study will be continued, and we discuss in another paper [18] the existence of a cooperative regime in which the transverse CBS perturbation would yield a squeezing of SBS quasi-solitons and *increase* their stability.

The authors thank Jean Botineau for many valuable discussions and comments.

Appendix A

We define the transverse profiles F for the optical mode, R for the high frequency axial acoustic mode ρ_a, M_n for the transverse acoustic mode ρ_n. r_max is the overall fiber radius.

$$B_n^{\Delta} = \frac{\int_0^{2\pi}\int_0^{r_\mathrm{max}} M_n^*(r,\varphi)\Delta_\perp\left(\left|F(r,\varphi)\right|^2\right) r\,\mathrm{d}r\,\mathrm{d}\varphi}{\int_0^{2\pi}\int_0^{r_\mathrm{max}}\left|M_n(r,\varphi)\right|^2 r\,\mathrm{d}r\,\mathrm{d}\varphi} \tag{A.1}$$

$$B^{\mathrm{SBS}} = \frac{\int_0^{2\pi}\int_0^{r_\mathrm{max}} R(r,\varphi)\left|F(r,\varphi)\right|^2 r\,\mathrm{d}r\,\mathrm{d}\varphi}{\int_0^{2\pi}\int_0^{r_\mathrm{max}}\left|F(r,\varphi)\right|^2 r\,\mathrm{d}r\,\mathrm{d}\varphi} \tag{A.2}$$

$$B^{\mathrm{CBS}} = \frac{\int_0^{2\pi}\int_0^{r_\mathrm{max}} M(r,\varphi)\left|F(r,\varphi)\right|^2 r\,\mathrm{d}r\,\mathrm{d}\varphi}{\int_0^{2\pi}\int_0^{r_\mathrm{max}}\left|F(r,\varphi)\right|^2 r\,\mathrm{d}r\,\mathrm{d}\varphi} \tag{A.3}$$

$$B_\mathrm{a} = \frac{\int_0^{2\pi}\int_0^{r_\mathrm{max}} R_n^*(r,\varphi)\left|F(r,\varphi)\right|^2 r\,\mathrm{d}r\,\mathrm{d}\varphi}{\int_0^{2\pi}\int_0^{r_\mathrm{max}}\left|R(r,\varphi)\right|^2 r\,\mathrm{d}r\,\mathrm{d}\varphi} \tag{A.4}$$

$$B^{\mathrm{Kerr}} = \frac{\int_0^{2\pi}\int_0^{r_\mathrm{max}}\left|F(r,\varphi)\right|^2 F(r,\varphi) r\,\mathrm{d}r\,\mathrm{d}\varphi}{\int_0^{2\pi}\int_0^{r_\mathrm{max}}\left|F(r,\varphi)\right|^2 r\,\mathrm{d}r\,\mathrm{d}\varphi}\,. \tag{A.5}$$

Appendix B

In order to homogenize the SBS coupling constants [1], we may define a longitudinal electrostrictive field E_a through:

$$\rho_\mathrm{a} = \mathrm{i}\left(\frac{4\varepsilon_0\rho_0 n^3}{cc_\mathrm{a}}\right)^{1/2} E_\mathrm{a}. \tag{B.1}$$

This reduces the pure SBS problem to only one coupling constant:

$$\kappa_\mathrm{a}^{\mathrm{SBS}} = \frac{\omega_\mathrm{p}}{4}\frac{\partial\varepsilon}{\partial\rho}\left(\frac{\varepsilon_0\rho_0}{cc_\mathrm{a}n}\right)^{1/2} \times B^{\mathrm{SBS}} B_\mathrm{a}\left[=\left(g_{\mathrm{SBS}}\frac{\gamma_\mathrm{a}\varepsilon_0 c^2}{4}\right)^{1/2}\right]. \tag{B.2}$$

Now, we introduce the dimensionless variables and the reduded coupling constants for the whole SBS-CBS problem (normalized with respect to $\kappa_\mathrm{a}^{\mathrm{SBS}}$ and the constant input pump E_p^0) as follows:

$$\tilde{E} = E_\mathrm{p}/E_\mathrm{p}^0;\quad \tau = t\kappa_\mathrm{a}^{\mathrm{SBS}}\left|E_\mathrm{p}^0\right|;\quad \xi = \frac{nz}{c}\kappa_\mathrm{a}^{\mathrm{SBS}}\left|E_\mathrm{p}^0\right|;$$
$$\mu_{\mathrm{e,a,n}} = \frac{\gamma_{\mathrm{e,a,n}}}{\kappa_\mathrm{a}^{\mathrm{SBS}}\left|E_\mathrm{p}^0\right|};\quad \tilde{\Omega} = \frac{\Omega}{\kappa_\mathrm{a}^{\mathrm{SBS}}\left|E_\mathrm{p}^0\right|} \tag{B.3}$$

$$Q = \rho_n\frac{(\kappa_\mathrm{a}^{\mathrm{SBS}})^2}{\kappa_{n\perp}} \tag{B.4}$$

$$K^{\mathrm{Kerr}} = \kappa^{\mathrm{Kerr}}\frac{\left|E_\mathrm{p}^0\right|}{\kappa_\mathrm{a}^{\mathrm{SBS}}} \tag{B.5}$$

$$K^{\mathrm{CBS}} = \frac{4cc_\mathrm{a}}{\omega_\mathrm{p}n^2}(\kappa_\mathrm{a}^{\mathrm{SBS}})^2\, B^{\mathrm{CBS}}\, B_n^{\Delta} \tag{B.6}$$

and obtain the quasi-1D 4-wave model:

$$\left[\partial_\tau + \partial_\xi + \mu_e\right]\tilde{E}_\mathrm{p} = -\tilde{E}_\mathrm{B}\tilde{E}_\mathrm{a} + \mathrm{i}\,K^{\mathrm{CBS}}\tilde{E}_\mathrm{p}Q + \mathrm{i}\,K^{\mathrm{Kerr}}\left(\left|\tilde{E}_\mathrm{p}\right|^2 + 2\left|\tilde{E}_\mathrm{B}\right|^2\right)\tilde{E}_\mathrm{p} \tag{B.7}$$

$$\left[\partial_\tau - \partial_\xi + \mu_e\right]\tilde{E}_\mathrm{B} = \tilde{E}_\mathrm{p}\tilde{E}_\mathrm{a}^* + \mathrm{i}\,K^{\mathrm{CBS}}\tilde{E}_\mathrm{B}Q + \mathrm{i}\,K^{\mathrm{Kerr}}\left(\left|\tilde{E}_\mathrm{p}\right|^2 + \left|\tilde{E}_\mathrm{B}\right|^2\right)\tilde{E}_\mathrm{B} \tag{B.8}$$

$$\left[\partial_\tau + \mu_\mathrm{a}\right]\tilde{E}_\mathrm{a} = \tilde{E}_\mathrm{p}\tilde{E}_\mathrm{B}^* + \tilde{f}_\mathrm{a} \tag{B.9}$$

$$\left[\partial_{\tau\tau} + 2\mu_n\partial_\tau + \tilde{\Omega}^2\right]Q = \left|\tilde{E}_\mathrm{p}\right|^2 + \left|\tilde{E}_\mathrm{B}\right|^2 + \tilde{f}. \tag{B.10}$$

References

1. J. Botineau, C. Leycuras, C. Montes, E. Picholle, J. Opt. Soc. Am. B **6**, 300 (1989)
2. C. Montes, D. Bahloul, I. Bongrand, J. Botineau, G. Cheval, A. Mahmoud, E. Picholle, A. Picozzi, J. Opt. Soc. Am. B **16**, 932 (1999)
3. R.W. Boyd, K. Rzazewski, P. Narum, Phys. Rev. A **42**, 5514 (1990)
4. I. Bar–Joseph, A.A. Friesem, E. Lichtman, R.G. Waarts, J. Opt. Soc. Am. B **2**, 1606 (1985)
5. A.L. Gaeta, R.W. Boyd, Int. J. Nonlinear Opt. Phys. **1**, 581 (1992)
6. C. Montes, A. Mamhoud, E. Picholle, Phys. Rev. A **49**, 1344 (1994)
7. S. Randoux, V. Lecœuche, B. Segard, J. Zemmouri, Phys. Rev. A **51**, R4345 (1995)
8. D. Yu, Weiping Lu, R.G. Harrison, Phys. Rev. A **49**, R24 (1994)
9. E. Picholle, C. Montes, C. Leycuras, O. Legrand, J. Botineau, Phys. Rev. Lett. **66**, 11 (1991)
10. C. Montes, A. Picozzi, D. Bahloul, Phys. Rev. E **55**, 1092 (1997)
11. S.P. Smith, F. Zarinetchi, S.E. Ezekiel, Opt. Lett. **16**, 393 (1991)

12. M. Nikles, L. Thevenaz, Ph.A. Robert, IEEE J. Lightw. Tech. **15**, 1842 (1997)
13. E.M. Dianov, A.V. Luchnikov, A.N. Pilipetskii, A.N. Starodumov, Opt. Lett. **15**, 314 (1990)
14. I. Bongrand, A. Picozzi, E. Picholle, Electron. Lett. **34**, 1769 (1998)
15. R.M. Shelby, M.D. Levenson, P.W. Bayer, Phys. Rev. B **31**, 5244 (1985)
16. A.B. Grunidin, D.J. Richardson, D.N. Payne, Electron. Lett. **29**, 1860 (1993)
17. A.N. Pilipetskii, E.A. Golovchenko, C.R. Menyuk, Opt. Lett. **20**, 907 (1995)
18. I. Bongrand, C. Montes, E. Picholle, J. Botineau, A. Picozzi, G. Cheval, D. Bahloul, Opt. Lett. **26**, 1475 (2001)
19. I. Bongrand, E. Picholle, submitted (2002)
20. A.J. Poustie, J. Opt. Soc. Am. B. **10**, 691 (1993)
21. A. Fellegara, A. Melloni, M. Martinelli, Opt. Lett. **22**, 1615 (1997)
22. Y. Jaouën, L. Du Mouza, Opt. Fiber Tech. **7**, 141 (2001)
23. A. Fellegara, S. Wabnitz, Opt. Lett. **23**, 1357 (1999)
24. Y. Hibino, T. Edahiro, T. Horigushi, Y. Azuma, N. Shibata, J. Appl. Phys. **66**, 4049 (1989)
25. A.N. Pilipetskii, A.V. Luchnikov, A.M. Prokhorov, Sov. Lightw. Commun. **3**, 29 (1993)
26. J. Botineau, private communication
27. E.L. Buckland, Opt. Lett. **24**, 871 (1999)
28. W.H. Glenn, IEEE J. Quant. Electron. **25**, 1218 (1989)
29. K. Bløtekjær, J. Light. Tech. **10**, 36 (1992)
30. W.M. Henry, Intern. J. Optoelectr. **7**, 453 (1992)
31. S. Fischer, P. Meyrueis, W. Schröder, Pure Appl. Opt. **5**, 55 (1996)
32. A. Fellegara, S. Wabnitz, Opt. Lett. **22**, 1615 (1997)
33. E. Picholle, A. Picozzi, Opt. Commun. **135**, 327 (1997)
34. A.M. Scott, K.D. Ridley, IEEE J. Quant. Electron. **25**, 438 (1989)
35. D.C. Johnson, K.O. Hill, B.S. Kawasaki, Radio. Sci. **12**, 519 (1977)